ISSN 0915-633X

NATIONAL INSTITUTE FOR FUSION SCIENCE

A Design Method of Divertor in Tokamak Reactors

N. Ueda, S.-I. Itoh, M. Tanaka and K. Itoh

(Received – July 27, 1990)

NIFS-36 Aug. 1990

RESEARCH REPORT
NIFS Series

NAGOYA, JAPAN

A Design Method Of Divertor In Tokamak Reactors

N. Ueda *, S. -I. Itoh+, M. Tanaka ** and K. Itoh+

* Mitsubishi Atomic Power Industries, Inc., Shibakouen, Minato-ku, Tokyo 105, Japan

\+ National Institute For Fusion Science, Nagoya 464-01, Japan

** Century Reserch Center Corp., Nihonbashi hon-cho, Chuo-ku, Tokyo 103, Japan

Keywords: tokamak reactor, divertor design, SOL, dense-cold plasma, erosion rate, baffle plate, fin plate, UEDA code.

Abstract

Computational method to design the efficient divertor configuration in tokamak reactor is presented. The two-dimensional code has been developed to analyze the distributions of the plasma and neutral particles for realistic configurations. Using this code, a method to design the efficient divertor configuration is developed. An example of new divertor, which consists of the baffle and fin plates, is analyzed.

§1 Introduction

The progress has been made in the design study of the fusion engineering reactor[1,2]. As a result of the quantitative estimations, it has been clear that the handling of the power and particle from the core plasma is one of the most important issues. The dominant part of the heat from the core which is carried by the charged particles is expected to flow to the divertor plate. The high heat flux must be removed from the plate. The erosion of the divertor plate must be minimized. At the same time, the Helium ash of the fusion reaction must be pumped out with proper speed of the pumping.

These requests are expected to be satisfied by employing the poloidal divertor configuration[3]. The concepts of the open, semi-closed and closed divertor configurations have been proposed. In these geometries, the dense and cold divertor plasmas can be maintained for some discharge conditions, satisfying the requests for the erosion rate, pumping speed, and shield for the impurity. The relation between the core plasma and the divertor conditions was analysed[4]. The key to satisfy the proper divertor function is the sufficient particle supply from the core plasma to the scrape-off layer (SOL) plasma. The more the particle is supplied, the lower the erosion rate becomes at the divertor plate. The progress of the knowledge on the core confinement has shown, however, the discharges with improved energy confinement are often associated with the better particle confinement, i.e., with the reduced particle flux to the SOL region[5]. At the same time, the better current-drive efficiency requires the operation at the lower density; this also means that the particle supply to the SOL region is reduced. The design of the efficient divertor configuration, which allows the divertor function for the wide region of the core plasma parameters, becomes an urgent task to design the experimental reactor. It is also noted that the requests for the divertor function can yield the trade-off. For instance, the request of the low erosion rate is satisfied by the high recycling at the plate. The high recycling rate can be realized by the baffle and fin plates which impede the escape of the neutral particles from the divertor region. Stopping neutrals, on the other hand, leads to the reduction of the conductance to the pumping duct. Therefore careful study on the configuration must be performed.

For the design of the divertor, the knowledge of the plasma and heat flow in the SOL region is inevitable. The analytic as well as numerical analyses have been developed to simulate the plasma in the SOL region[6-10]. The two-dimensional and time dependent code (UEDA code) has been developed to study the plasma behavior in the SOL region for the given supply of the particle and energy from the core plasma[9, 10]. This code enables us to relate the core plasma condition and divertor condition in a realistic geometry. Based on this code, we, in this article, present a method to design the divertor structure and configurations for the FER grade tokamak. The method utilizes two types of the numerical computation and analytic estimation. The simple code solves the neutral particle motion in the given and fixed plasma distribution in a realistic geometry assuming the

azimuthal symmetry. By changing the shapes of the wall, baffle pates, divertor plates and pumping ducts, the conductance of neutral particles to the pumping duct is calculated. This procedure yields crude estimates for the enhancement factor of the flux near the divertor plate and the conductance to the pump. Choosing a proper example configuration from this simplified model, we solve the plasma and neutral particles in a consistent manner by the UEDA code.

The second section explain the framework of the design method. In section 3, an example is shown, which employs a fin structure. The comparison with the standard design which employes a flat divertor plate is presented. The summary and discussion are presented in section 4.

§2 Method of the divertor design

We consider the FER grade tokamak, which has the poloidal divertor configuration (see Fig. 1). We first discuss the design criteria. The evaluation function is presented. The metod is then discussed.

2.1 Evaluation function

The conditions the divertor must satisfy are as follows. (1) The erosion rate is low and the source of the impurities must be suppressed. (2) Neutral pressure is high enough so that the efficient pumping is possible with small pumping duct. (3) The partial pressure of the Helium is high. (4) The conductance to the pumping duct is high. (5) The back flow of neutrals to the core plasma is small. (6) The flow of the impurities to the core plasma is low.

The key parameter to determine the erosion rate is the electron temperature in front of the divetor plate, T_{div}. The erosion rate as a function of the energy of incident ions is presented in the Appendix. The incident energy E_i, is related to T_{div} as an approximate relation, $E_i=5T_{div}$[11]. The sputtering yield ratio has a strong energy dependence (see Fig. A1 in Appendix). The ion energy for the large sputtering yield ratio ($>10^{-3}$) ranges from ~30eV (low Z material) to~200eV (high Z material). This puts the upper limit for the electron temperture in front of the divertor plate.

The high recycling divertor is the solution to reduce T_{div}[4-9]. The ratio of the mean free path of neutral particles for the ionization, λ_m, to the width of the divertor plasma Δ, is important to establish the dense divertor plasma. If this ratio is small, the chain reaction of the ionization and resultant increment of the particle flux onto the divertor plate, Γ_{div}, occurs. The mean free path depends on the plasma parameters strongly. This dependnce is tabulated in the Appendix explicitly. Because the chain reaction of the ionization can increase the plasma density, and this increment of the density further reduce the mean free path of the ionization. Due to these complicated relation between the plasma production and the neutral motion, careful calculation of

the plasma and neutrals under a realistic geometry is requested.

By this localized ionization, the enhancement factor of the particle flux, $G = \Gamma_{div}/\Gamma_{out}$ (Γ_{out} is the particle supply from the core plasma to the SOL region), increases. The heat flux is proportional to $T_{div}\,\Gamma_{div}$, and the particle flux scales to $n_{div}\sqrt{T_{div}}$.[4] Keeping the particle and energy supply to the SOL plasma fixed, the G-dependence of T_{div} is estimated. The temperature T_{div} is expected to scale to 1/G, and n_{div} to $G^{1.5}$, assuming that the heat channel width does not change. The enhancement factor G strongly increases as the particle supply reaches critical value. From these reasons, the cold and dense divertor plasma condition requires lower limit for Γ_{out} (or the upper bound for the energy supply to the divertor plasma Q_{div}). The energy flux to the divertor plate, Q_{div} is given by $(Q_{out} - Q_{remote})$, where Q_{out} is the power supply from the core plasma and Q_{remote} is the loss due to the atomic processes in the SOL region. The energy loss owing to the atomic process consists of the ionization, excitation and radiation. The dependence on the plasma parameter of these losses are also given in the Appendix. The table of the atomic and molecular processes which should be employed in the design is also given in the appendix.

The quantitative calculation has been performed by use of the two-dimensional code and employing these processes. The region of the discharge conditon, which gives the divertor function, was obtained. Fig. 2 illustrates one example. The better design of the divertor implies that the dense and cold divertor plasma establishes for the wider range of the core plasma parameters, i. e. in the smaller Γ_{out} and larger Q_{out}.

Next point is the efficiency of the pumping. The necessary pumping velocity is determined from the request that the source of the helium atoms due to the fusion reaction balances with those pumped at the pumping duct. The source is given by the power of the reactor. The request for the pumping speed at the pumping duct is relaxed if the neutral helium density is high at the duct. The necessary pumping velocity to sustain the fusion reaction rate at the given power is one of the evaluation function.

The divertor plasma is known to have the ability to retain impurities from invading into the core plasma. In the case where the heat and particle mainly intract with material at the divertor plasma, the erosion of the plate is the main source of impurities. The reduction of the errosion is, as is discussed, realized by reducing T_{div}. The shield of the impurity flow is also necessary, because small but finite value of the erosion cannot be eliminated. The impurity flow along the field line is determined by the balance between the drag force due to the ion flow to the plate and thermal force which is in the direction to the core. The ratio of the impurity influx into the core plasma to the source flux from the plate is the index of the impurity shielding.

2.2 Method of design

The evaluation of these quantities requires to solve the plasma and neutral particles in realistic wall and plasma boundaries. To perform this calculation, the unified edge divertor analysis code (UEDA code) has been developed[9, 14] and applied to analyze experimental data.[9, 10, 13] We explain how the code is used in optimizing the divertor design.

Althogh the code predicts the consistent solution for plasma and neutrals, the code uses substantial CPU time. Some simplification would be desirable. The logic of the analysis is as follows.

The wide survey on the shape of the divertor region (wall, baffle, fin plates) are performed using a simplified stand-alone code. This code solves the neutral particle motion for the given plasma distribution employing the atomic processes with Monte-Carlo calculations. By using this code, the ratio of the ionization, η_i, that of the charge exchange, η_{cx}, that to return to the main plasma, η_m, and that for the pumping, η_p, are calculated. The plasma distribution is assumed fixed and is given according to the scaling law, which has been established by the selfconsistent calculations[4, 9, 10] for a particular configurations. This calculation is not selfconsistent, because the plasma is fixed. However, the first calculation by the code gives rough estimations on the parameters η_i, η_{cx}, η_m, and η_p. The value η_i is related to the flux amplification factor G, i.e., $1/G \approx 1-\eta_i$. The conservation relation

$$\eta_i + \eta_m + \eta_p = 1$$

holds. The dense and cold divertor condition requires large G, i. e., large η_i. The high conductance to the duct is realized if η_p is high. The objective to use the stand-alone code is to find the geometrical configurations (such as baffle plate and fin plate) which have high η_i and η_p. The reduction of η_m is essential, because the large neutral flow to the main plasma often deteriorates the energy confinement time of the core plasma.

By this procedure, the target design of the plates are selected. We next confirm the performance by running the UEDA code in the geometry. In running the UEDA code, the plasma and neutral particles are soved selfconsistently. The evaluations on the key parameters, i. e., T_{div}, heat deposition channel width, erosion rate, neutral pumping velocity, impurity invasion and the neutral back flow to the core plasma, are calculated. The selection of the divertor configuration is confirmed, and the operation region for the core plasma parameters is obtained.

§3 Example of the design

We study the model of the divertor design for the FER grade plasma. The size of the plasma is as follows; the major radius R=4.6m, the minor radius a = 1.2m, the elongation ratio of the crossection is 1.8. The magnetic field is chosen as B=4.5T at the axis. Plasma current is chosen as I_p = 15MA.

The power and particle supply from the core plasma is chosen as Q_{out} = 60MW and Γ_{out}=3x10^{23}/sec. The divertor plate material is chosen to be W, and the Marlow model of neutral particle reflection is used [12]. Helium content is assumed to be 7% of Γ_{out} at the plasma edge. The value of Γ_{out} is fairly small and may put a severe condition for the divertor. The choice is made in the motivation to find the lower limit of the particle supply from the core.

For these parameters the UEDA code is run under the boundary condition of Fig. 1 which includes the conventional divertor configuration. This calculation gives the standard parameter to evaluate the divertor function. In the calculation, we assume that the parallel conductivity is given by the classical value and the perpendicular one is anomalous. As an example, we choosen the Bohm-like parameter as D = D_B/2, κ =2nD_B (D_B is the Bohm diffusion coefficient, T_e/16eB). The coefficients 1/2 and 2 are used according to the comparison study[9].

The code empoyes the fluid model for the plasma behavior, which consists of the continuity equation for the density, the momentum conservation equation governing the parallel velocity $\upsilon_{\parallel}$, the diffusion equation for the perpendicular velocity υ_{ψ} and the energy conservation equations for the electron and ion temperature Te and Ti. The explicit form of the fluid equations and the boundary conditions employed are written in ref.[9, 14] and are not repeated here.

The result of the conventional configuration is shown in Fig. 3. The plasma temperatue in front of the divertor plate, T_{div}, reaches to ~80eV. The plasma density in the outer divertor region becomes ~4.5x10^{20}/m^3 on the flux tube of j = 7; this flux tube is about 20cm distant along the plate from the separatrix magnetic surface at the divertor plate. The errosion rate reaches 4.4cm/year. This maximum value appears on the j = 10 flux tube, which is adjacent to the separatrix. The peak value of the heat flux to the plate is 0.9kW/cm^2. The pumping rate of fuel ions is found to be about 4x10^{22}/sec, i. e., the pumping efficiency η_p reaches 13%. This number is for the fuel particles. The Helium exhaust is also calculated. The pumping rate reaches to 2x10^{20}/sec. This result shows a sufficient ability for the ash exhaust. In a steady state of burinng, the heat flow to the SOL plasma of 60MW corresponds to 60Q/(5+Q) MW of the α-particle heating, where Q is the power enhancement factor. This power is originated from the generation of the α-particles at the rate of about Q/(5+Q)x10^{20}/sec. In the range of Q ≃ 10, this source is below

10^{20}/sec. The neutral back flow to the core plasma is negligibly small. It is also noted that the He particle flux onto the outer divertor plate reaches to $3x10^{21}$/sec. The contour of the radiation loss in the divertor region is given in Fig. 3. 4. The peak value reaches ~100 MW/m^3, and the total remote radiation cooling reaches ~20MW. This value is still too small for the purpose of substantially reducing the heat flux onto the divertor plate.

The result of the standard configuration is found to have an efficient pumping ability. However, the maximum temperature reaches ~80eV and the erosion rate is 4.4cm/y. Further inclination of the target plate to the magnetic flux surfacer might lead to the reduction of the heat flux and the erosion rate, still this value of the erosion rate (4.4cm/y) is unacceptable from the design criteria. In order to reduce the erosion rate of the divertor plate, we will examine other type of the structure. One way to reduce the temperature is, as is discussed in §2, the increment of the ionization rate in the divertor region. This would be realized by baffling the neutral flow, i. e., by the fin plates. The fin plate near the divertor plate was applied for the helical plasma and found to increase the recycling rate and reduce the erosion rate, i. e., to extend the operation regime of the core plasma[13]. The result is compared to the standard case.

The blow-up figure of the divertor region is given in Fig. 4. Compared to the standard divertor (a), the fin structure is added (b). The height is denoted by d and the angle is characterized by θ. The fin plate is located expecting that the plasma temperature at the head is low enough and the erosion is negligible. The fin plate is expected also to work for the tokamak reactor. The point is to find the condition that the plasma temperature is reduced and the pumping efficiency is increased without increasing the neutral flow to the main plasma.

According to the procedure described in §2, we first analyze the problem empoying the stand alone code. The parameter survey is done over the various values of θ and d. The evaluation is given on the points that the parameters η_i and η_p are enhanced while η_m is kept low.

The plasma parameters are given in the stand-alone code according to the results of the standard divertor plate, Fig. 3. As the height of the fin increases, the ionization probability increases. This is because that the neutral particles reflect at the fin and enter the SOL plasma again. Associated with this change, the probability to reach the pumping duct, η_p, would be reduced. The increment of η_i is associated with the reduction of η_p. If θ becomes large, then the reduction of η_p becomes slower. If θ becomes too large, the enhancement of the value η_i is not expected. In other words, the amplification factor G does not increase, and the proper region in (Q_{out}-Γ_{out}) space does not extend. We compute the stand-alone code for the geometry of Fig. 4. The results from the stand-alone code are shown in Fig. 5. The distribution of the neutral particle is compared. In the case of the standard geometry, Fig. 4 (a), the neutral particles are spread over the divertor region and the pumping duct. On the contrary, the high density region is formed in

front of the plate for the case of the fin structure: at the same time the neutral density in the pumping duct is reduced. This means that the dense and cold divertor condition may be easily established for the fin structure, but the pumping efficiency would be sacrificed.

In order to evaluate the performance of the fin structure, the UEDA code is also run for the case of Fig. 4 (b). The device parameters, Q_{out}, Γ_{out} from the core and the transport coefficient and other calculational conditions are chosen common to the standard case. The high divertor plasma temperature is moderated in the case of the fin configuration. Fig. 6 illustrates the case of the geometry of the fin plate. The divertor plasma temperature reduces to $T_{div} = \underline{47eV}$ in this case. According to the scaling study[4], T_{div} is known to scale approximately as Γ^{-1}. Based on this scaling, we note that the reduced temperature allows the reduction of the particle supply from the core Γ_{out} (i. e., the operation of the core plasma in the low density region). The lower bound of Γ_{out} to keep T_{div} constant is reduced approximately by the factor of about 2. The neutral recycling becomes very strong in this case. The erosion rate is reduced to 2.7cm/y associated with the reduction of the temperature. The peak value of the heat flux increases to 1.9kW/cm^2. The fin plate reduces the pumping velocity. the pumping rate of fuel ions is about 10^{22}/s, i. e., the efficiency reduces to about 3% for the fuel ions. The exhaust of Helium ash also becomes difficult. The pumping rate of He atoms is below 10^{20}/sec. We observe that the α-particles move along the flux tube in the SOL region in the poloidal direction. Helium particles finally reach the inside divertor plate. The He particle flux onto the divertor plate is about 2×10^{22}/sec for the inside divertor and less than 10^{21}/sec for the outside divertor plate. Comparing to the standard case, the condensation of the He particle flux onto the divertor plate is increased for the inside divertor. This implies that the He particles must be pumped from the <u>inside divertor region</u>.

It is noted that the fin plate is not so effective as in the case of much smaller device.[13] This is because the peak position of the heat flux shifts from that of the particle flux on the divertor plate because of the perpendicular diffusion. This shift becomes ~10cm (measured in the direction perpendicular to the magnetic surface), which is longer than the mean free path of neutrals for the dense cold divertor plasma. Hence the fin plate can enhance the particle flux onto the divertor plate in the flux tube of large particle flux, but does not affect much the flux tube with large energy flux. This is because the neutral particles emitted from the plate are ionized before reaching the region of high energy flux tube. This may cast a new problem in the future large devices. One possible resolution may be given by introducing a local gas puffing to the flux tube with large heat flux. The active control of the divertor region will be discussed in a separate article.

The enhancement of the ionization near the fin plate may cause a strong heating of the fin plate by the change exchange particles. The energy flux to the fin plate is also calculated. It is confirmed that the erosion of the fin plate does not cause a new problem.

§4 Summary and Discussion

In this article, the method of the physical design of the efficient divertor structure is discussed. The proposed method utilizes a set of numerical code and analytic estimation. Example is presented for the FER grade tokamak reactor. A fin plate is introduced and the increment of the working region for the core plasma is discussed. This new structure can reduces the plasma temperature by the expense of the reduced pumping efficiency. If the pumping is realized near the inside divertor plate, the choice of the fin improves the over all divertor function. On the other hand, if the pumping speed is more critical than the erosion rate, the standard case is a better candidate compared to the fin case.

The stand-alone code is used to perform the survey over a wide range of geometry. The approximate shape is selected. The selfconsistent code is then solved and the divertor function is examined quantitatively. By this system of codes, the various shapes are examined and the final solution is obtained by the selfconsistent calculation.

The UEDA code utilizes the transport coefficients of the SOL plasma. The result depends on the choice of the transport model. For example, the Bohm-like model is used. The data base for the transport coefficient is, however, sparse and needs further verification. If the better modelling for the SOL transport would be found, then the optimum design would be changed. In such a situation, the design should be performed again, using the new data base and this system of the codes.

Acknowlegements

Authors acknowledge continuous encouragements by Drs. S. Iwai (Mitsubishi Atomic Power Ind. Inc.), H. Fujita (Mitsubishi Fusion Centre) and A. Iiyoshi (NIFS). Part of this work is supported by the Grant-in-Aid for Scientific Research of Ministry of Education, Japan.

Appendix : Design data base

In this appendix we list the numerical data, which are usually used in the design of the divertor.

[A] Sputtering yield ratio

Fig. A1 illustrates the sputtering yield ratio of C and W. Reduction of the plasma temperature in front of the divertor plate below ~5ev for C and ~40eV for W is required to avoid fatal damage of the plate. (quoted from ref. [15])

[B] Ionization mean free path

In the design of the divertor, it is important to take into account the "ionization mean free path" of the neutral particle. Tabe A1 shows the dependence of the mean free path (cm) on the plasma parameters. It should be noted the mean free path depends strongly on the plasma parameters, Te (ev) and N_e ($1/cm^3$).

[C] Radiation loss by atomic and molecular processes

The energy loss associated with the atomic and molecular processes are also important for the establishment of the dense cold divertor plasma. The plasma loses, energy through the excitation and ionization of neutral particles. The temperature dependence of the loss rate is given in Fig. A2 This loss rate shows its peak in the low temperature region. Once the temperature is reduced, then the loss rate increases rapidly and tends further reduce the plasma temperature. (quoted from ref. [16]).

[D] Ionization reaction rate

The reaction rate of electron impact ionization of hydrogen including the effects of multi-step ionization is listed in Fig. A3. The reaction rate also has a strong dependence on the plasma parameter. (quoted from ref. [16]).

[E] Dominant plasma/neutral reactions

The set of neutral/plasma reaction included in the code is listed in Table A2 for hydrogenic and helium atoms and molecules. (quoted from ref. [16]).

References

[1] ITER Team, ITER Concept Definition (ITER Documentation Series, No. 3), (IAEA, Vienna, 1989).

[2] FER Team, to be presented in the 13th International Conference on Controlled Thermonuclear Fusion Research (1990, Washington).

[3] S. Yoshikawa and A. Iiyoshi, Introduction to Nuclear Fusion (Baihu-kan, 2nd edition, 1976) 124 (in Japanese)

[4] S. -I. Itoh, N. Ueda, K. Itoh, Plasma Physics Controlled Fusion 32 (1990), in press.

[5] S. -I. Itoh, et al., Kakuyugo Kenkyu, 63 (1990) in press (in Japanese).

[6] F. Wagner and K. Lackner, in Physics of the Plasma Wall Interactions in Controlled Fusion (ed. D. E. Post and R. Behrisch, NATO ASI Series B131, Plenum Press, 1984) 931.

[7] M. Petravik, D. Post, D. Heifetz J. Schmidt, Phys. Rev. Lett. 48 (1982) 326.

[8] B. J. Braams, P. J. Harbour, M. F. a. Harrison, E. S. Hotston, J. G. Morgan, J. Nucl. Mater., 128 & 129 (1984) 75.

[9] N. Ueda, M. Kasai, M. Tanaka et al, Nucl. Fusion 28 (1988) 1183.

[10] N. Ueda, K. Itoh, S.-I. Itoh, Nucl. Fusion 29 (1989). 173.

[11] J. Wesson, in Tokamaks (Oxford, 1987)

[12] O. S. Oen and M. T. Robinson, Nuclear Instruments and Methods 132 (1976) 647-653.

[13] N. Ueda, K. Itoh, S.-I. Itoh, Jpn. J. Appl. Phys. 28 (1989) 2597.

[14] N. Ueda and M. Tanaka, J. Nucl. Science Technology 27 (1990) 106.

[15] D. Smith, in Ninth Symp. of Eng. Problems of Fusion Reseach (IEEE, New York, 1981) Vol. 1, 719-722.

[16] D. B. Heifetz, in Physics of Plasma Wall Interactions in Controlled Fusion (ed. D. E. Post and R. Behrisch, Plenum Press, 1986) 695.

Figure captions

Fig. 1 Model geometry and mesh of the SOL and divertor region for the experimental reactor.The orthogonal z(i) - ψ(i) co-ordinates system is employed. z(i) and ψ(j) denotes the poloidal length of the magnetic line of force and the poloidal flux, respectively. i stand for the index in the poloidal direction and j denotes the magnetic flux tube number. j = 10 correspnds to the flux tube which is adjacent to the separatrix line. Section $\overline{AB}$ denotes the entrance of the down-pipe. 4% of the neutral particles which enter into the section is pumped in the simulation.

Fig. 2 Example of the region of the dense-cold divertor plasma in JFT-2M.
The region of the dense-cold divertor plasma on (Γ_{out} - Q_{out}) space is illustrated. The symbol "◊" denotes the calculated point and the cold plasma (T_{div} < 30eV) is established below the line shown in the figure (quoted from ref. 4.).

Fig. 3.1 The profiles in the poloidal direction for each flux tube (—— : j = 10, —— : j = 9, ----- : j = 8, —·— : j = 7).
The left end points correspond to the temperature at the outer divertor and right one for inner divertor.

Fig. 3.2 Ne profiles in the poloidal direction for each flux tube. This figure shows that the peak of Ne at the outer divertor exists at j = 7 flux tube.

Fig. 3.3 Divertor temperature and density profiles along the outer divertor plate. (A - A') denotes the length along the plate (see also Fig. 4-a). This figure clearly indicates that the peak of Te exists at the j = 10 flux tube which locates adjacent to the separatrix line on the plate. On the contrary, the peak of n_e locates at about 23cm distant from the sepatrix line. This is the reason for the low recycling and resultant high divertor temperature (~80eV) at the j = 10 flux tube.

Fig. 3.4 2-D power loss profile in the divertor region (a : $10^8 w/m^3$, b : 0.5 x $10^8 w/m^3$, c : $10^7 w/m^3$, d : 0.5 x $10^7 w/m^3$, e : $10^6 w/m^3$, f : 0.5 x $10^6 w/m^3$).
The peak of the power loss in the outer divertor also locates at the j = 7 flux tube.

Fig. 3.5 Profiles for the heat flux, particle flux and erosion rate along the outer divertor plate (—— : particle flux, —·— : heat flux, -----: erosion rate). The particle flux is also dominant at the j = 7 flux tube but the peak of the heat flux locates at the j = 10 flux tube. This separation of the peak position of these fluxes cause the high tempeture at the j = 10 flux tube (~80eV) and resultant peak erosion rate (~4.4cm/y).

Fig. 4 Blow-up of the divertor region. (a) is the standard divertor and (b) for the fin type divertor.

Fig. 5 Comparison between the neutral density for the standard divertor (a : 2.5 x $10^{19}/m^3$, b : 2.5 x $10^{18}/m^3$, c : 2.5 x $10^{17}/m^3$, d : 2.5 x $10^{16}/m^3$) and the fin type divertor (a: 2 x $10^{19}/m^3$, b : 1.6 x $10^{19}/m^3$, c : 1.3 x $10^{19}/m^3$, d : 2.5 x $10^{18}/m^3$, e : 2.5 x $10^{17}/m^3$, f : 2.5 x $10^{16}/m^3$).
The neutral density near the plate at the j = 10 flux tube for the standard divertor (a) is about 3 x $10^{17}/m^3$. On the contrary, more than 2.5 x $10^{18}/m^3$ is expected for the fin type divertor at the corner of the wedge.

Fig. 6.1 Te profiles in the poloidal direction of the fin type divertor (—— : j = 10, —— : j = 9, ----- : j = 8, —·— : j = 7).
It is noted that the result for the fin type divertor is performed under the fixed plasma parameters obtained from the selfconsistent analysis in (a).
This figure shows the divertor temperature at the j = 10 flux tube is reduced to Te ~ 47eV by the fin structure (see also Fig. 3.1).

Fig. 6.2 Ne profiles in the poloidal direction for the fin type divertor.
The maximum divertor density exists at the j = 10 flux tube. This is because of the high recycling of the fuel ions by the fin structure (see also Fig. 3.2).

Fig. 6.3 2-D profile of the neutral density for the fin type divertor calculated selfconsistently by the UEDA code (a : 2.5 x $10^{18}/m^3$, b : 2.5 x $10^{17}/m^3$, c : 2.5 x $10^{16}/m^3$).
This result should be compared with that of stand-alone code (Fig. 5-b).

Fig. 6.4 Divertor temperatue and density profiles along the outer divertor plate for the fin type divertor (see also Fig. 3.3).

Fig. 6.5 2-D power loss profile in the divertor region for the fin type divertor (a : 10^8w/m^3, b : 0.5 x 10^8w/m^3, c : 10^7w/m^3, d : 0.5 x 10^7w/m^3, e : 10^6w/m^3, f : 0.5 x 10^6w/m^3). The peak loss exists at the corner of the wedge (see also Fig. 3.4).

Fig. 6.6 Profiles for the heat flux, particle flux and erosion rate along the outer divertor plate for the fin type divertor plate (—— : particle flux, —·— : heat flux, ----- : erosion rate). In this case the peak of these fluxes and erosion rate exist at the j = 10 flux tube (see also Fig. 3.5).

Fig. A1 Ion impact sputtering yield ratio as a function of incident particle energy for C and W.

Fig. A2 Average electron energy loss for each electron-impact ionization of hydrogen including excitation/de-excitation process, as a function of electron temperature and density.

Fig. A3 Rate coefficient for electron impact ionization of hydrogen, including excitation and de-excitation processes.

Table A1 Dependence of the mean free path on the plasma parameters.

Table A2 Dominant neutral/plasma reactions

Fig. 1

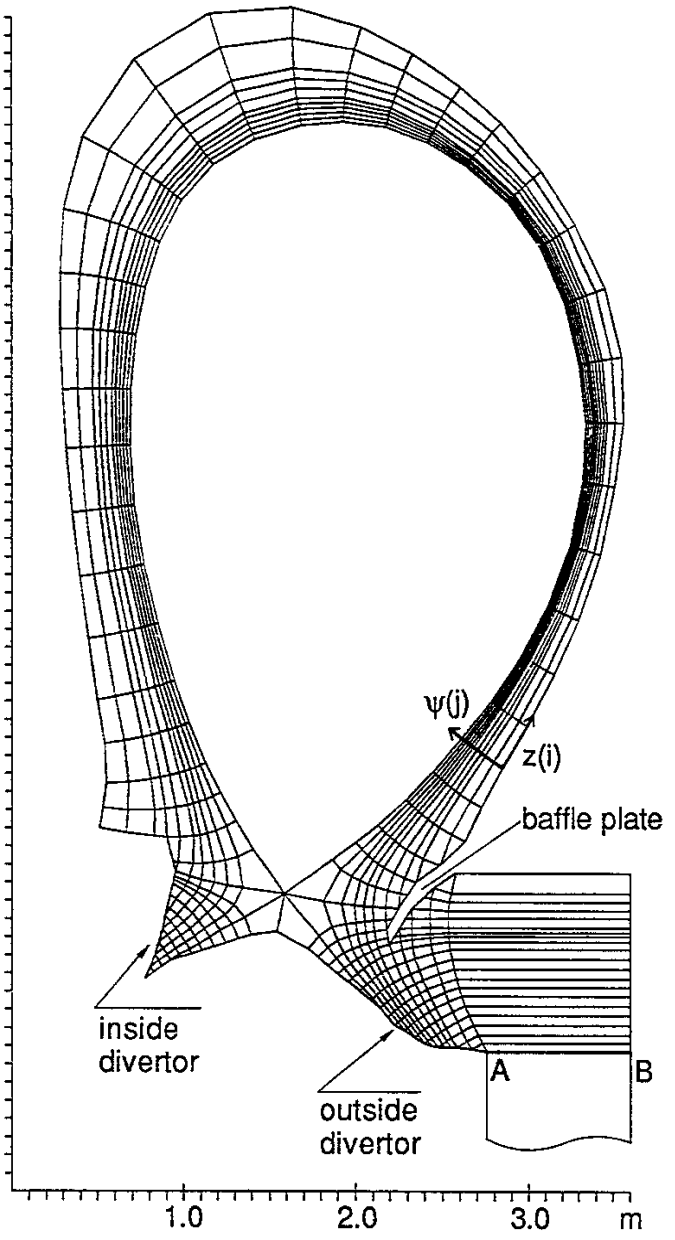
ψ(j)
z(i)
baffle plate
inside
divertor
outside
divertor
A
B
1.0
2.0
3.0
m

Fig. 2

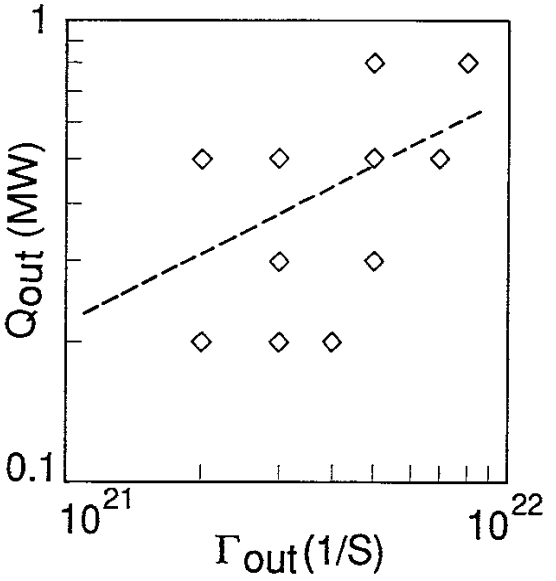

Fig. 3.1

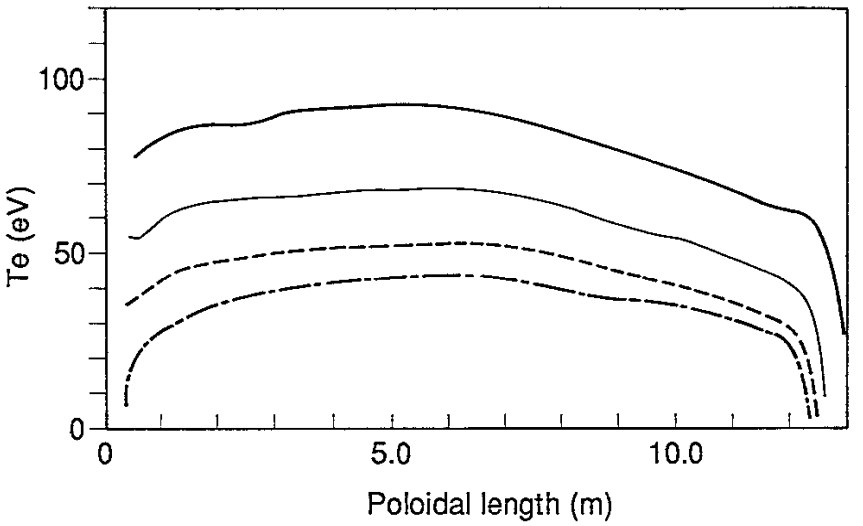

Fig. 3.2

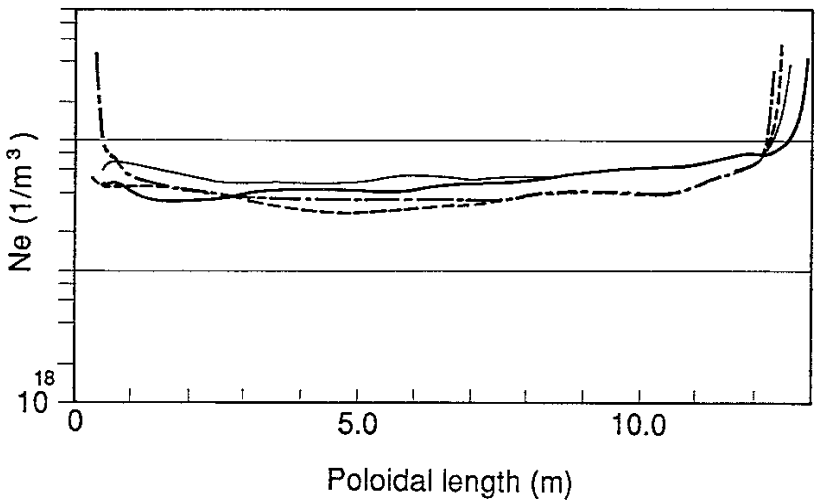

Fig. 3.3

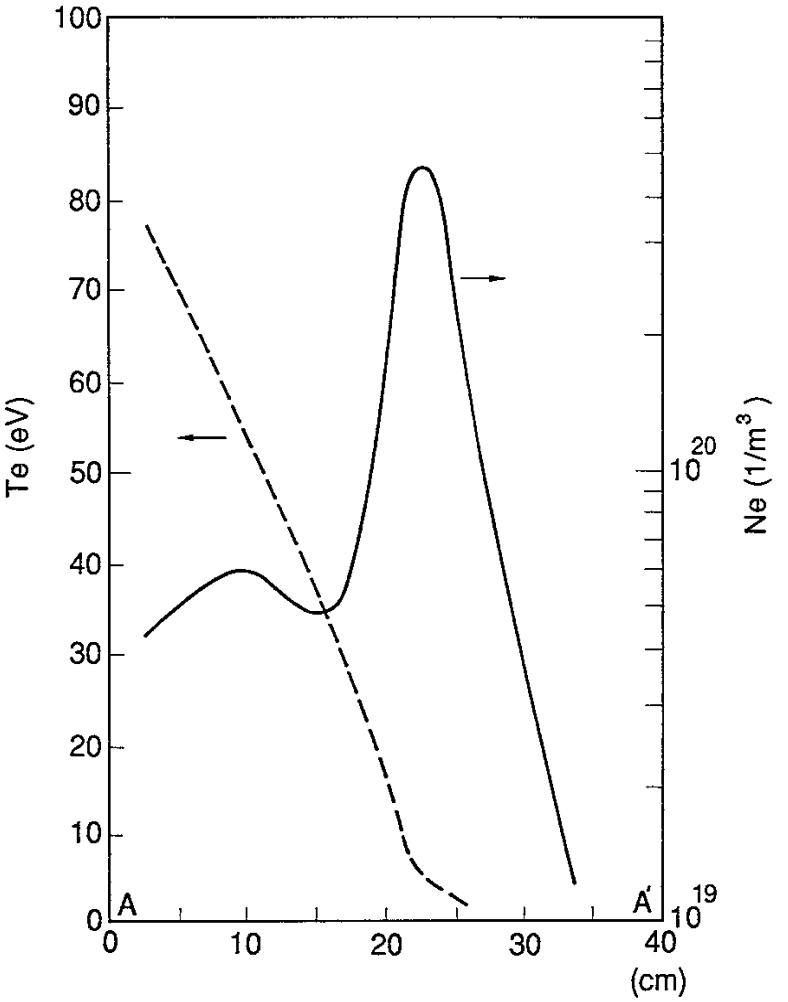
100
90
80
70
60
50
40
30
20
10
0
Te (eV)
A
A'
0
10
20
30
40
(cm)
10^{20}
10^{19}
Ne ($1/m^3$)

Fig. 3.4

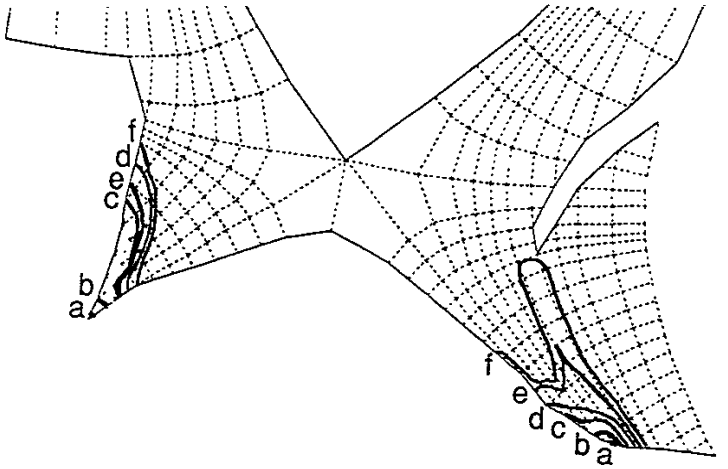

Fig. 3.5

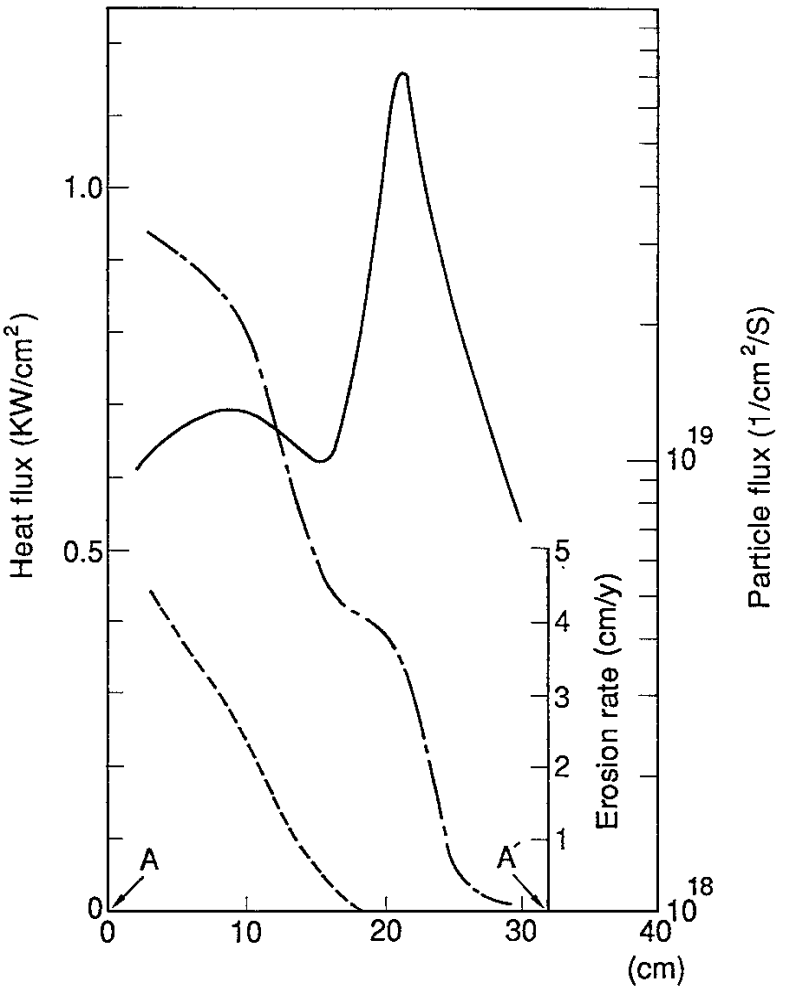
Heat flux (KW/cm^2)
1.0
0.5
0
A
A´
0
10
20
30
40
(cm)
Erosion rate (cm/y)
5
4
3
2
1
Particle flux (1/cm^2/S)
10^{19}
10^{18}

Fig. 4

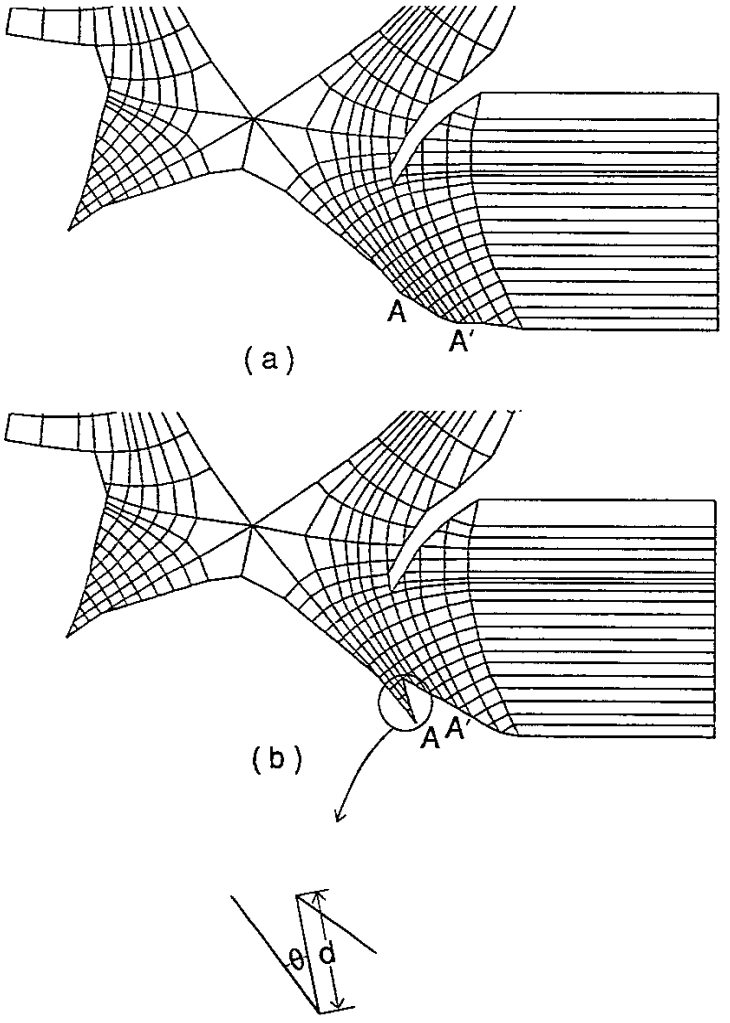

Fig. 5

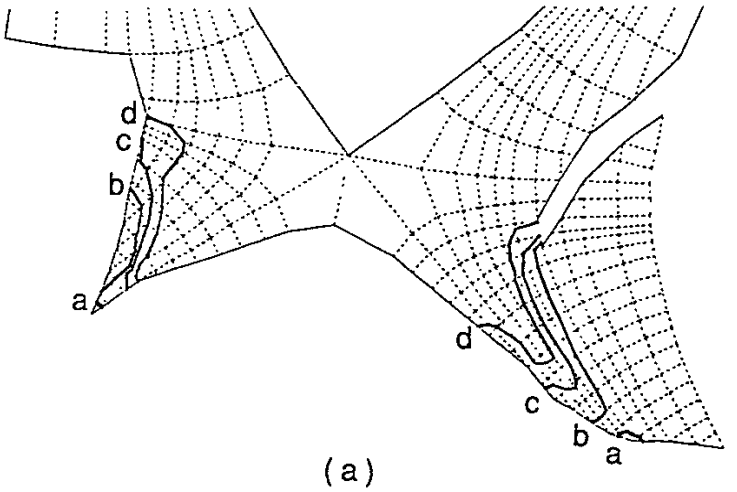

(a)

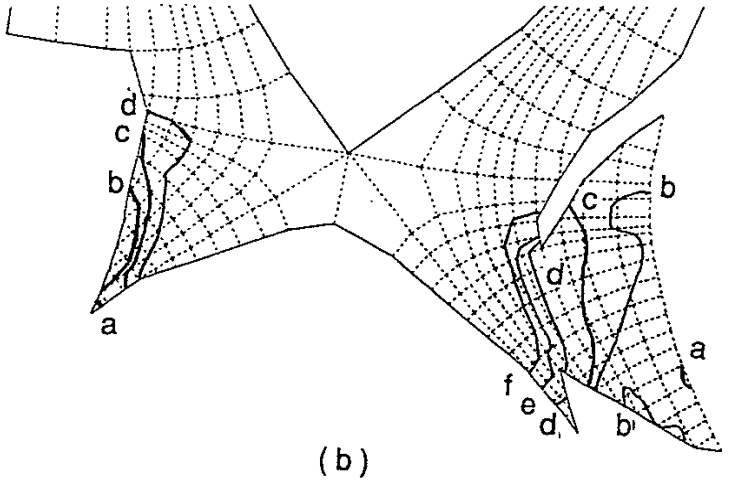

(b)

Fig. 6.1

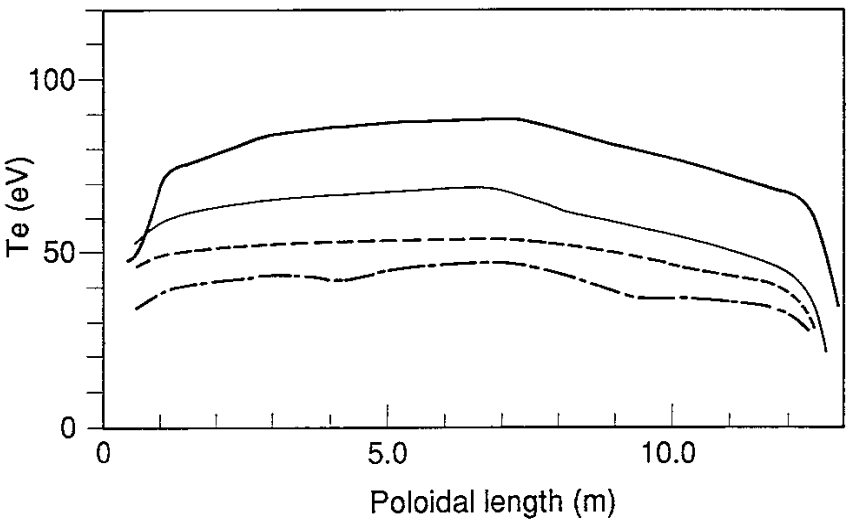

Fig. 6.2

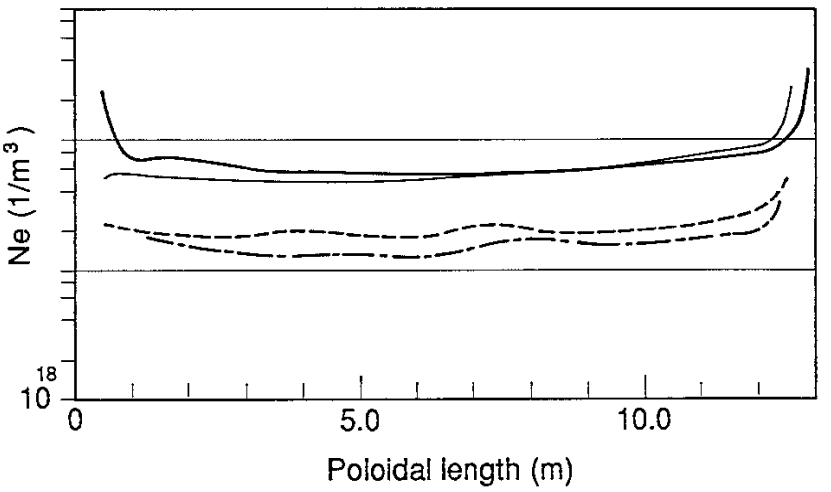

Fig. 6.3

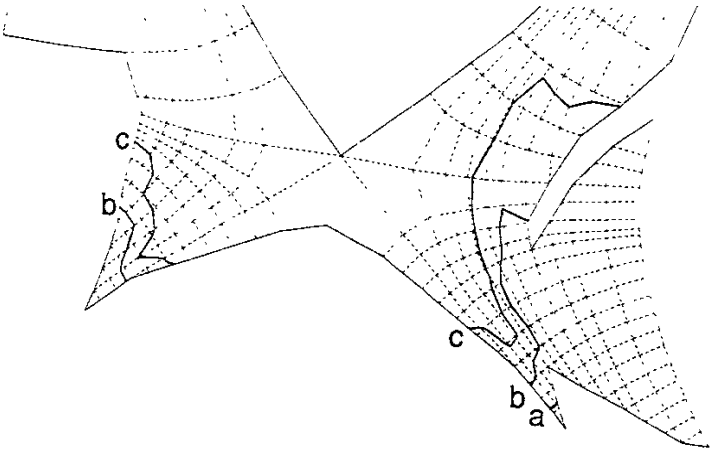

Fig. 6.4

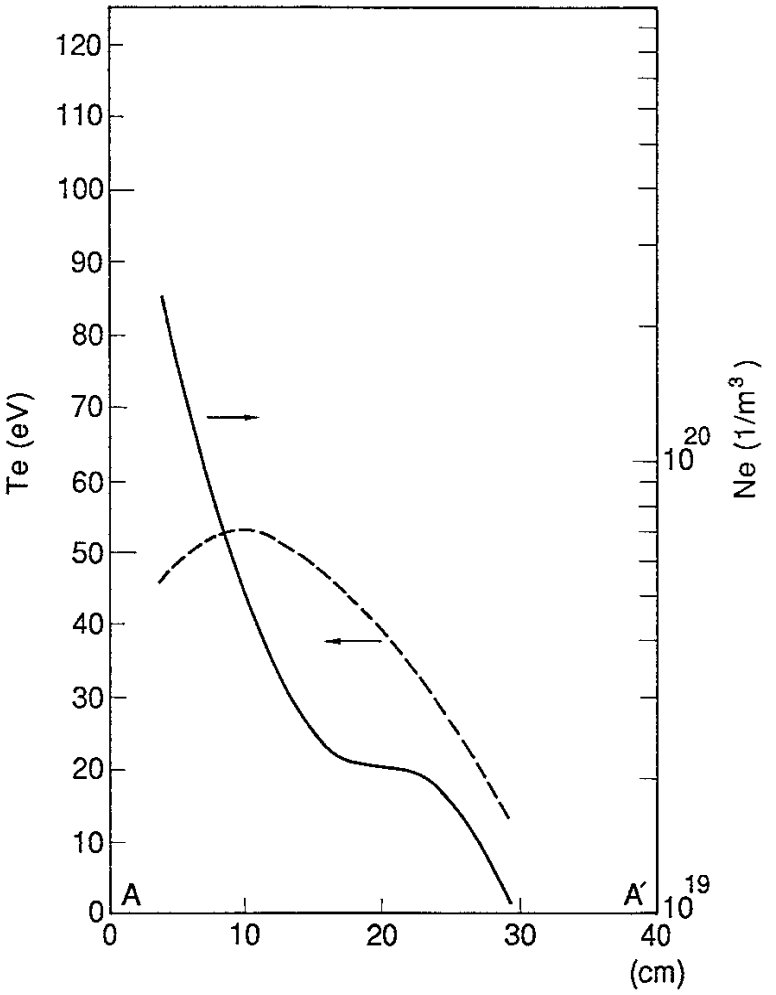
120
110
100
90
80
70
60
50
40
30
20
10
0
Te (eV)
A
A'
0
10
20
30
40
(cm)
10^{20}
10^{19}
Ne (1/m^3)

Fig. 6.5

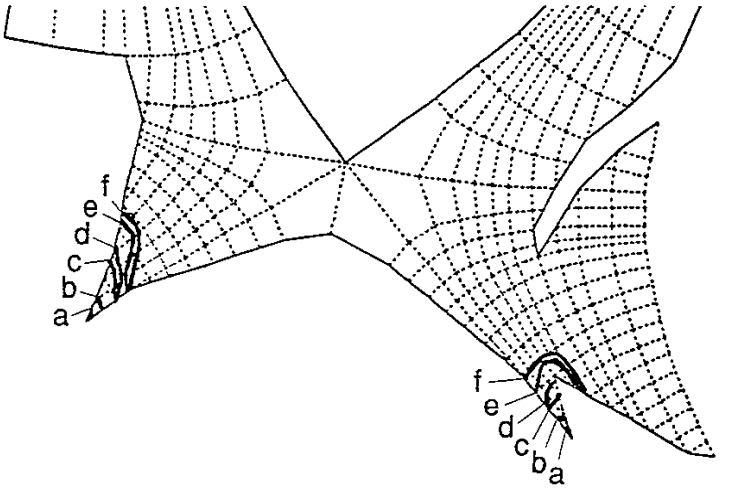

Fig. 6.6

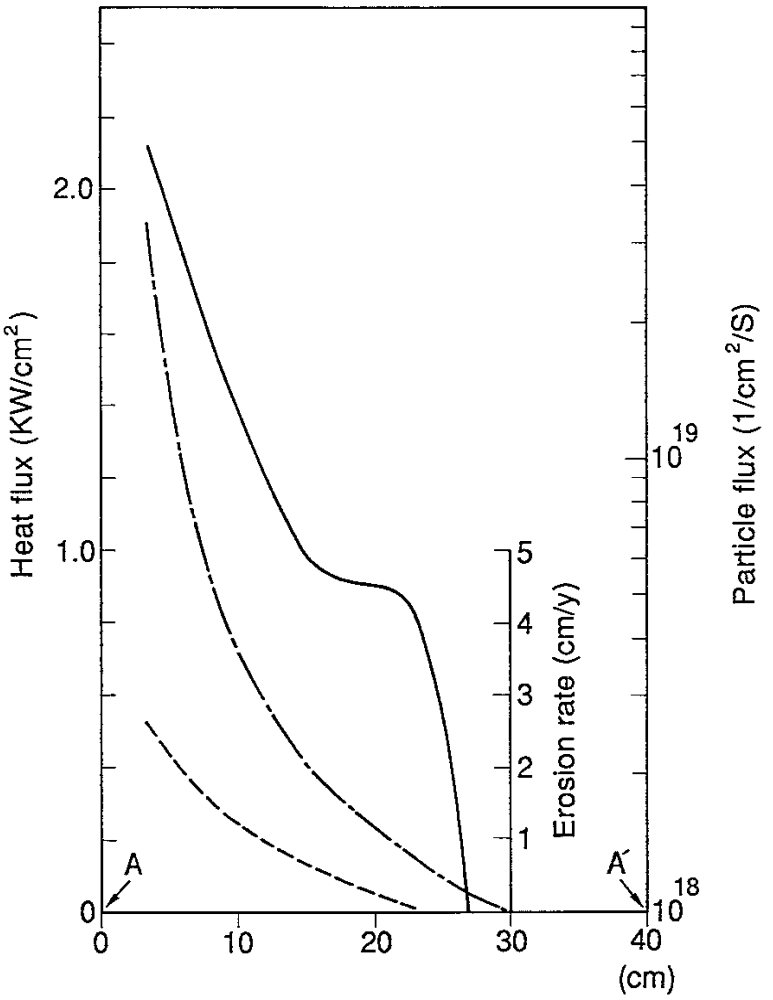
Heat flux (KW/cm²)
2.0
1.0
0
A
A'
0
10
20
30
40
(cm)
Erosion rate (cm/y)
5
4
3
2
1
Particle flux (1/cm²/S)
10¹⁹
10¹⁸

Fig. A1

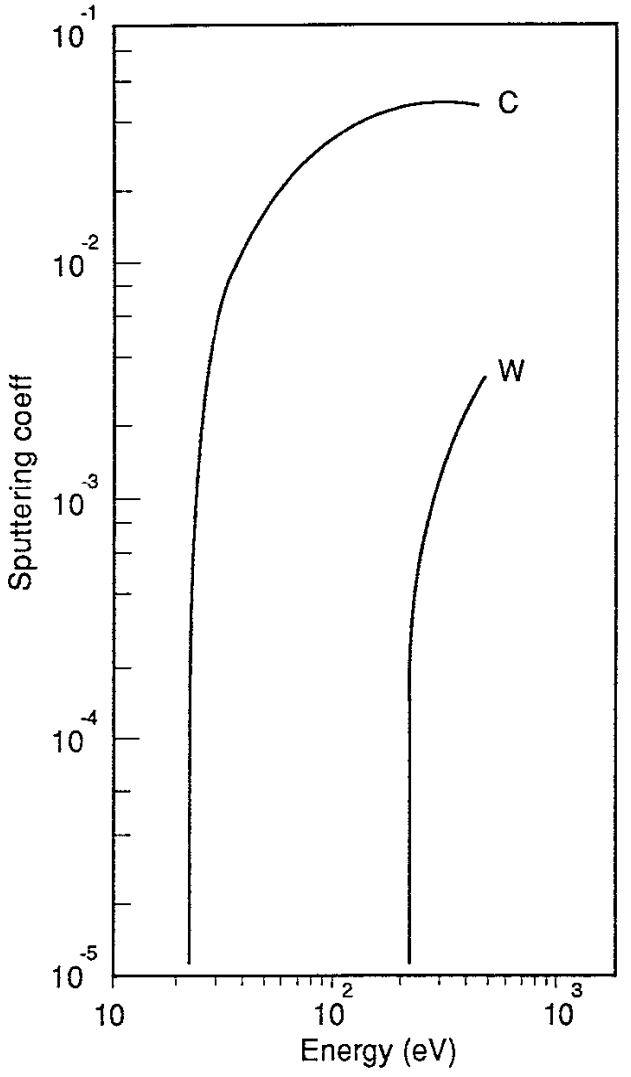

Fig. A2

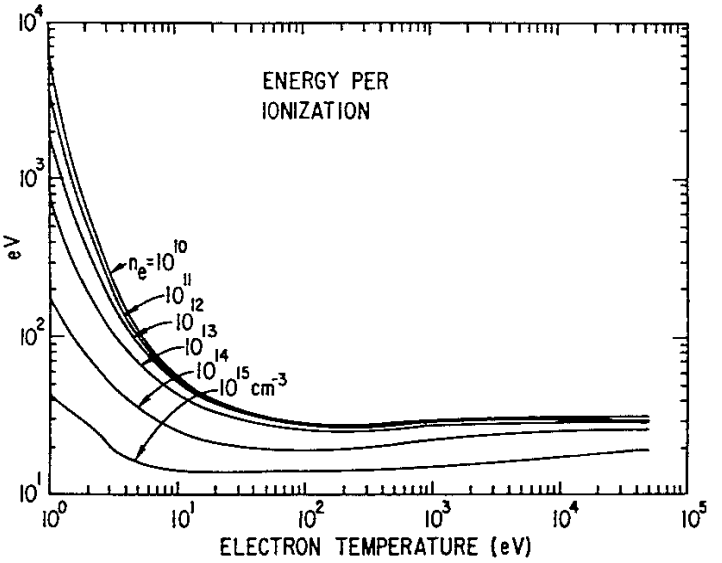
ENERGY PER
IONIZATION
eV
$n_e=10^{10}$
10^{11}
10^{12}
10^{13}
10^{14}
10^{15} cm^{-3}
ELECTRON TEMPERATURE (eV)

Fig. A3

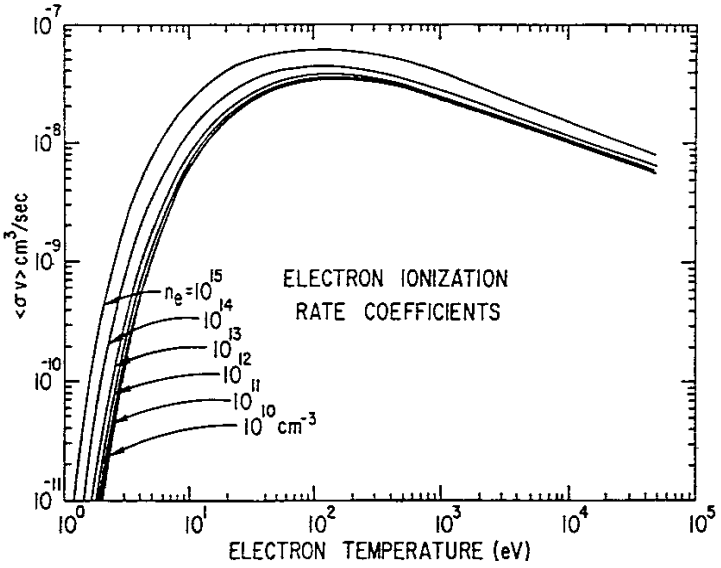
ELECTRON IONIZATION
RATE COEFFICIENTS
$n_e = 10^{15}$
10^{14}
10^{13}
10^{12}
10^{11}
10^{10} cm^{-3}
$\langle \sigma v \rangle$ cm^3/sec
ELECTRON TEMPERATURE (eV)

Table A1

Te \ Ne	10^{12}	5×10^{12}	10^{13}	5×10^{13}	10^{14}	5×10^{14}	10^{15}
1	4.4×10^{7}	4.5×10^{6}	1.7×10^{6}	1.1×10^{5}	3.8×10^{4}	2.1×10^{3}	6.9×10^{2}
2	8.2×10^{4}	1.1×10^{4}	4.4×10^{3}	4.0×10^{2}	1.5×10^{2}	1.1×10^{1}	4.3
3	9.5×10^{3}	1.4×10^{3}	6.0×10^{2}	6.6×10^{1}	2.5×10^{1}	2.3	9.2×10^{-1}
4	3.5×10^{3}	5.5×10^{2}	2.4×10^{2}	2.9×10^{1}	1.2×10^{1}	1.2	4.8×10^{-1}
5	1.9×10^{3}	3.1×10^{2}	1.4×10^{2}	1.8×10^{1}	7.3	8.0×10^{-1}	3.3×10^{-1}
6	1.2×10^{3}	2.0×10^{2}	9.3×10^{1}	1.3×10^{1}	5.2	6.0×10^{-1}	2.5×10^{-1}
7	8.7×10^{2}	1.5×10^{2}	7.0×10^{1}	9.9	4.1	4.9×10^{-1}	2.1×10^{-1}
8	7.1×10^{2}	1.2×10^{2}	5.8×10^{1}	8.3	3.5	4.3×10^{-1}	1.8×10^{-1}
9	5.8×10^{2}	1.0×10^{2}	4.8×10^{1}	7.2	3.1	3.9×10^{-1}	1.6×10^{-1}
10	5.1×10^{2}	9.2×10^{1}	4.3×10^{1}	6.5	2.8	3.6×10^{-1}	1.5×10^{-1}
20	2.9×10^{2}	5.4×10^{1}	2.6×10^{1}	4.3	1.9	2.7×10^{-1}	1.2×10^{-1}
30	2.6×10^{2}	4.9×10^{1}	2.3×10^{1}	4.0	1.8	2.7×10^{-1}	1.2×10^{-1}
40	2.5×10^{2}	4.8×10^{1}	2.3×10^{1}	4.0	1.9	2.8×10^{-1}	1.3×10^{-1}
50	2.6×10^{2}	4.9×10^{1}	2.4×10^{1}	4.2	1.9	3.0×10^{-1}	1.3×10^{-1}
60	2.6×10^{2}	5.0×10^{1}	2.5×10^{1}	4.3	2.0	3.1×10^{-1}	1.4×10^{-1}
70	2.7×10^{2}	5.2×10^{1}	2.6×10^{1}	4.5	2.1	3.3×10^{-1}	1.5×10^{-1}
80	2.8×10^{2}	5.4×10^{1}	2.7×10^{1}	4.7	2.2	3.5×10^{-1}	1.6×10^{-1}
90	2.9×10^{2}	5.7×10^{1}	2.8×10^{1}	5.0	2.3	3.7×10^{-1}	1.7×10^{-1}
100	3.1×10^{2}	5.9×10^{1}	2.9×10^{1}	5.2	2.4	3.9×10^{-1}	1.8×10^{-1}
150	3.7×10^{2}	7.1×10^{1}	3.5×10^{1}	6.3	3.0	4.8×10^{-1}	2.2×10^{-1}
200	4.3×10^{2}	8.3×10^{1}	4.1×10^{1}	7.4	3.5	5.7×10^{-1}	2.6×10^{-1}
250	4.9×10^{2}	9.5×10^{1}	4.7×10^{1}	8.5	4.0	6.5×10^{-1}	3.0×10^{-1}
300	5.5×10^{2}	1.1×10^{2}	5.3×10^{1}	9.6	4.6	7.4×10^{-1}	3.4×10^{-1}

Table A2

Charge-exchange (H is any hydrogenic species):

$$H^0 + H^+ \rightarrow H^+ + H^0$$
$$He^0 + He^{+(+)} \rightarrow He^{+(+)} + He^0$$
$$He^0 + H^+ \rightarrow He^+ + H^0$$

Electron-impact ionization:

$$e^- + H^0 \rightarrow H^+ + 2e^-$$
$$e^- + He^0 \rightarrow He^+ + 2e^-$$
$$e^- + H_2^0 \rightarrow H_2^+ + 2e^-$$

Electron dissociation:

$$e^- + H_2^0 \rightarrow 2H^0 + e^-$$
$$e^- + H_2^0 \rightarrow H^0 + H^+ + 2e^-$$
$$e^- + H_2^+ \rightarrow 2H^0$$
$$e^- + H_2^+ \rightarrow H^0 + H^+ + e^-$$
$$e^- + H_2^+ \rightarrow 2H^+ + 2e^-$$

Recombination:

$$H^+ + e^- \rightarrow H^0$$